Flat 410 and 660 Dicontinuities beneath Northeastern Japan: Implication for a Sub-Slab Wet Plume Hypothesis

K. Miyazaki[1], and J. Nakajima[1]

[1]Earth and Planetary Sciences, School of Science, Tokyo Institute of Technology, Tokyo, Japan

Corresponding author: Kazuki Miyazaki (miyazaki.k.ak@m.titech.ac.jp)

Key Points:

- The tomography of the 410 and 660 beneath northeastern Japan is using receiver function analysis
- The depths of the 410 and 660 are not correlated with a marked sub-slab low-velocity anomaly
- The sub-slab low-velocity anomaly can be interpreted as representing hydrous effect rather than high temperature

Abstract

Recent seismic tomography studies have shown that distinct low-velocity anomalies exist below subducting slabs in many subduction zones and these anomalies are interpreted as a hot plume from the lower mantle. However, how high the temperatures in the sub-slab low-velocity anomalies are still unclear. Here, we conduct receiver function analysis and estimate the horizontal temperature variation in the mantle transition zone by determining the depth variation of 410 and 660 discontinuities beneath northeastern Japan. The obtained results show that the depth of the two discontinuities changes little, which suggests no distinct thermal heterogenies over the study area. Therefore, we infer that the major cause of the sub-slab low-velocity anomaly is attributable not to high-temperature anomaly but to the presence of small amount (~0.2 wt%) of hydrous minerals, which can explain the sub-slab low-velocity anomalies and the flat 410 and 660 discontinuities.

Plain Language Summary

Recent studies suggested that the seismic low-velocity zones exist under the subducting slab in many subduction zones. This low-velocity zones are interpreted as a hot upwelling flow from the lower mantle. However, how high the temperatures in this plume are still unclear. Here, we conduct receiver function analysis and estimate the depth variation of 410 and 660 seismic velocity discontinuities beneath northeastern Japan. The 410 and 660 discontinuities are associated with the phase transformations from olivine to wadsleyite at 410 km depth and from ringwoodite to bridgmanite at 660 km depth, respectively. Since the depths of the two discontinuities are sensitive to the temperature variations in the mantle transition zone, precise estimation of the depths of the 410 and 660 discontinuities can provide quantitative estimation of the thermal anomaly. The obtained results shows that the depth of the two discontinuities changes little, which suggests no distinct thermal heterogenies over the study area. Therefore, we infer that this low-velocity zone reflects wet upwelling flow rather than hot upwelling flow.

1 Introduction

Recent seismic tomography analyses have shown the existence of distinct low-velocity anomalies beneath subducting slabs in many subduction zones (Fan and Zhan 2021), including Japan (Asamori and Zhao 2015; Liu and Zhao 2016a; Liu and Zhao 2016b), South America (Portner et al., 2017; Lee et al., 2023), Cascadia (Hawley et al., 2016; Bodmer et al., 2018; Zhao and Hua, 2021; Liang et al., 2023), and Sumatra subduction zones (Huang et al., 2015). Geodynamic modeling of plate subduction and mantle convection suggests that the sub-slab low-velocity anomalies reflect the downwelling asthenosphere materials originating either from a weak, buoyant layer under the oceanic lithosphere (Hawley et al., 2016) or from hotspot materials entrained by slab subduction (Portner et al.,2017; Bodmer et al., 2018; Zhao and Hua 2021). In contrast, Dai et al. (2023) have shown a local uplift of the 660 discontinuity beneath the Cascadia subduction zone using receiver function (RF) analysis and suggested that the sub-slab low-velocity anomaly reflects upwelling hot materials from the lower mantle.

Many tele-seismic tomography analyses have shown the existence of a distinct low-velocity anomaly beneath the Pacific plate of northeastern Japan, which is continuously distributed from at least 1100 km depth to ~200 km depth (Zhao 2004; Obayashi et al., 2006; Zhao 2009; Wei et al. 2012; Asamori and Zhao 2015; Wei et al. 2015; Liu and Zhao 2016a; Liu and Zhao 2016b; Wei et al., 2016). Since there are no hotspots around the Japanese Islands, the

sub-slab low-velocity anomalies are interpreted to reflect the hot upwelling mantle induced by the collapsing of the stagnant Pacific slab into the lower mantle (Zhao 2004; Zhao 2009). Obayashi et al. (2006) suggested that the sub-slab low-velocity anomaly at 410 km depth can be explained by the increases in temperatures by ~200 K. The temperature increase by ~200 K is comparable to that of hot materials originating from the lower mantle and entrained toward the 410 discontinuity, which is simulated by geodynamic modeling (Morishige et al., 2010). If the sub-slab low-velocity anomaly is produced by the thermal origin as high as 200 K, the 660 would be elevated by ~15 km given the Clapeyron slope of -3.2~-2.6 MPa/K (Akaogi et al.,2007; Muir et al., 2021). However, the elevation of the 660 has not yet been confirmed by seismological observations.

This study conducts RF analysis using a large number of tele-seismic waveforms recorded at a dense seismological observation network in Japan to constrain the depth variations of the sub-slab 410 and 660 discontinuities. Since the 410 and 660 are associated with the phase transformations from olivine to wadsleyite and from ringwoodite to bridgmanite, respectively, the depths of the two discontinuities are sensitive to the temperature variations in the mantle transition zone. Therebefore, precise determination of the depths of the 410 and 660 can provide quantitative estimation of the thermal anomaly, which enhances our understanding of the sub-slab mantle dynamics.

2 Data and Method

We examined 1086 events with Mw ≧ 5.5 that occurred between April 2005 to March 2023 (Fig 1a). Waveforms of these earthquake were recorded at 455 Hi-net stations (Fig 1b) operated by the National Research Institute for Earth Science and Disaster Prevention (NIED). The natural frequency of seismometer is 1 Hz and waveform data are recorded with a sampling frequency of 100 Hz. After correcting for the instrument response to the waveform with the method of Maeda et al. (2011), we applied a band-pass filter (0.1-15 Hz) to the observed waveform. In the Fourier transformation, we used a time window of 163.84 s, starting 40 s before the theoretical P-wave arrival time. RFs were calculated by deconvolving the radial and transverse components from vertical components with a water level of 0.001 and a low-pass filter at 0.5 Hz. We discarded RFs with <3 signal-to-noise ratios, and finally obtained a total of 216,414 RFs. RFs were migrated into a space-domain using iasp91 1D velocity model (Kennett and Engdahl 1991) with the Vectorial Receiver Function Method (Kawakatsu and Watada 2007; Kawakatsu and Yoshioka 2011) that considers the three-dimensional refraction on the dipping surface of the Pacific slab by correcting for incident and azimuthal angles of RFs. We set a 10 km (horizontal) × 2 km (depth) grid along four profiles sub-parallel to the strike of the Japan trench (Fig 1a) and employ a common conversion point stacking along each profile. We then gathered Ps amplitudes within 100 km width from each profile to produce cross-sectional images of RFs.

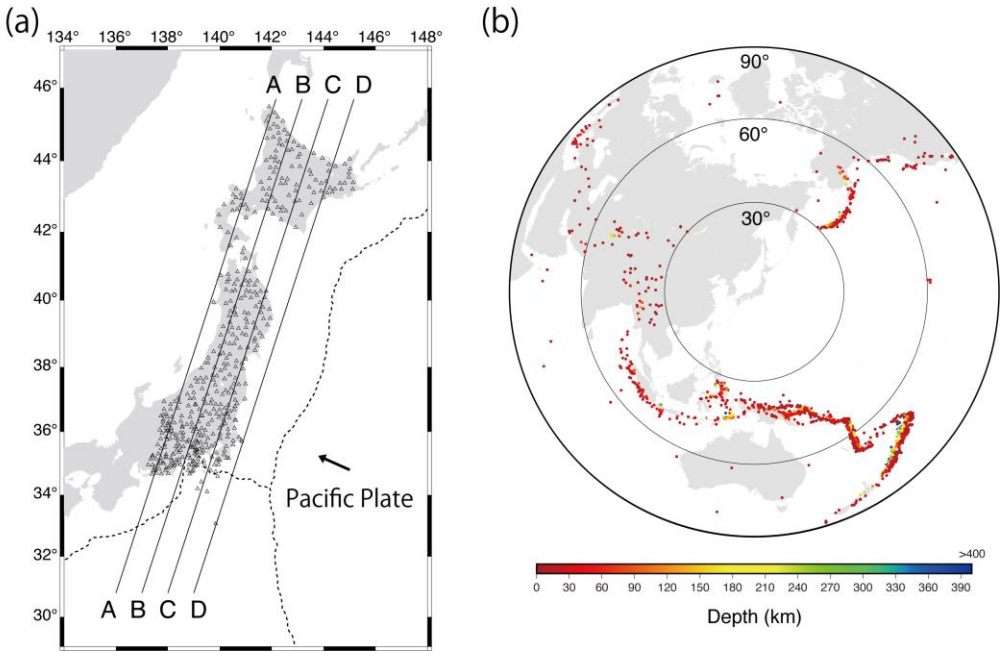

Figure 1. (a) Locations of Hi-net seismometers (triangles) used in this study and four profiles A, B, C and D along which we obtained receiver function images. Four line (A–D) are profiles along which we display RF imaging in Figure 2. The dotted line represents trenches and troughs. (b) Epicenter distribution of tele-seismic events used in this study. The color scale shows the focal depth of earthquakes.

3 Results

We observed two clear planes of positive amplitudes at ~410 km and ~660 km depths, which are interpreted as the 410 and 660 discontinuities, respectively (Fig 2a). Of note, the 410 and 660 are almost flat with no large depth variation for all profiles, even though the 660 in the southern end of profiles A-C depress locally by 30-40 km. The local depression at ~660 km is considered to be the effect of the subducting cold Pacific slab (Tonegawa et al., 2005).

To quantify the depth variation of the 410 and 660 obtained by RF analyses, we identified the depth of the maximum positive amplitudes within a depth range of ±40 km from each of 410 and 660 km depth. We defined the discontinuity depths at horizontal distances of every 50 km (crosses in Fig 2a). The obtained result confirms that the discontinuity depths are nearly constant, and the depth variations in each of the two discontinuities are estimated to be less than ~ 10 km along all profiles (Fig 2b).

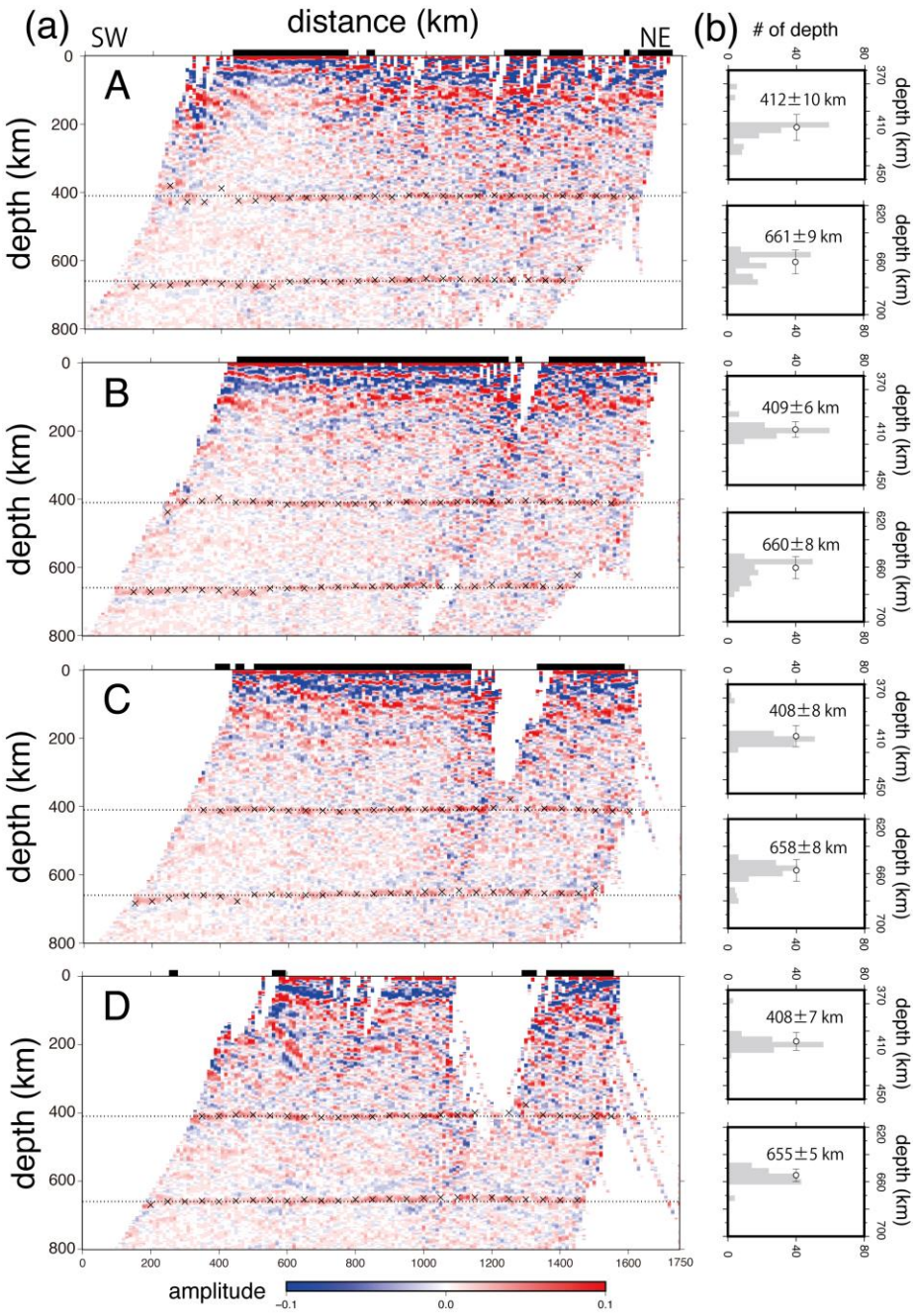

116 **Figure 2**. (a) The receiver function images along profile A, B, C, and D. Grids with more than
117 250 RF stacks are shown, where red and blue indicate positive and negative amplitudes,
118 respectively. The dotted lines indicate 410 km and 660 km depth. Black bar on the top represents
119 the land area. The cross marks represent the depths of discontinuity determined from the
120 maximum amplitudes of RFs over a horizontal span of 100 km and displayed every 50 km. (b)
121 Histograms representing the depths of 410 discontinuity (upper panel) and 660 discontinuity
122 (lower panel).
123

We performed a bootstrap test to evaluate the stability and robustness of the depths of the 410 and 660. For each set of RFs, we created 200 data subsets, with each subset derived from the same number of RFs with a random resampling of the original RF data set. The result of the bootstrap test shows that the standard deviation of the depths of the 410 and 660 are both less than 2 km (Fig S1), demonstrating that the depth of the 410 and 660 km can be constrained with high accuracy.

We also assessed the effect of different velocity models on the obtained RFs images, where we carried out the same analysis using two additional different velocity models, PREM (Dziewonski et al. 1981) and AK135 (Kennett et al. 1995). The obtained results yielded almost the same depth variations in the 410 and 660 for the three velocity models, suggesting that our results are robust regardless of assumed 1D velocity models. However, the absolute depths of the 410 and 660 are changed by ~10 km and ~20 km, respectively for the different velocity models (Fig S2). Therefore, we focuse on the relative depth variation of the 410 and 660 along the profiles to discuss the origin of the sub-slab low-velocity anomaly.

4 Discussion

According to recent seismic tomography analysis, velocity perturbations of the sub-slab low-velocity anomaly are estimated to be –2~–1 % for P waves (Obayashi et al. 2006; Wei et al. 2012; Wei et al. 2015; Liu and Zhao 2016) and –3~–2 % for S waves (Asamori and Zhao 2015; Wei et al., 2015; Liu and Zhao 2016a,b). Almost all the tomographic models show that the sub-slab low-velocity anomaly has the depth extent of 100-150 km and extends horizontally at least 1000 km in the along-arc direction. The S-wave velocity model obtained by Asamori and Zhao (2016) clearly demonstrates the existence of an inverted V-shaped sub-slab low-velocity anomaly in the mantle transition zone (Fig 3).

If the sub-slab low-velocity anomaly reflects only the thermal effect, then the temperature is required to be elevated by 200–300 K using the temperature-velocity relations of dlnVp/dT = 0.5– 1%/100K and dlnVs/dT = ~1%/100K in the mantle transition zone (Anderson and Isaak, 1995; Civiero et al., 2019). Such high temperature anomalies would result in the depression by 25–35 km for the 410 and the uplift by 25–35 km for the 660, given Clapeyron slopes of +3 MPa/K (Bina and Helffrich 1994; Akaogi et al., 2007) at 410 km and –2.6 MPa/K (Akaogi et al.,2007) or –3.2 MPa/K (Muir et al., 2021) at 660 km.

Fig 4 shows the relationship between the relative topography of the 410 and 660 and S-wave velocity perturbation by Asamori and Zhao (2015), which are sampled every 50 km in the horizontal distance along profiles B and C (crosses in Fig 2a and Fig 3). Although Obayashi et al. (2006) suggested a temperature increase by ~200 K to explain the ~32.5 km depression of the 410, it is evident from Fig 4 that the 410 is almost flat and there are no correlations between the 410 and 660 topography and S-wave velocity perturbations. Our results strongly suggests that the sub-slab low-velocity anomaly cannot be explained by the high temperature anomaly only. It is noted that the RF imaging in this study does not incorporate a 3D velocity model when we convert RFs from the time domain to the depth profile. However, if we consider the local effect of the sub-slab low-velocity anomaly to produce the depth profile of RFs, the 410 would become shallower than those derived with the 1D model. Such shallow 410 contradicts the effect of high-temperature anomaly, whereby we could conclude that the high temperature is not the major cause of the sub-slab low-velocity zone even if the 3D velocity model is involved in the analysis.

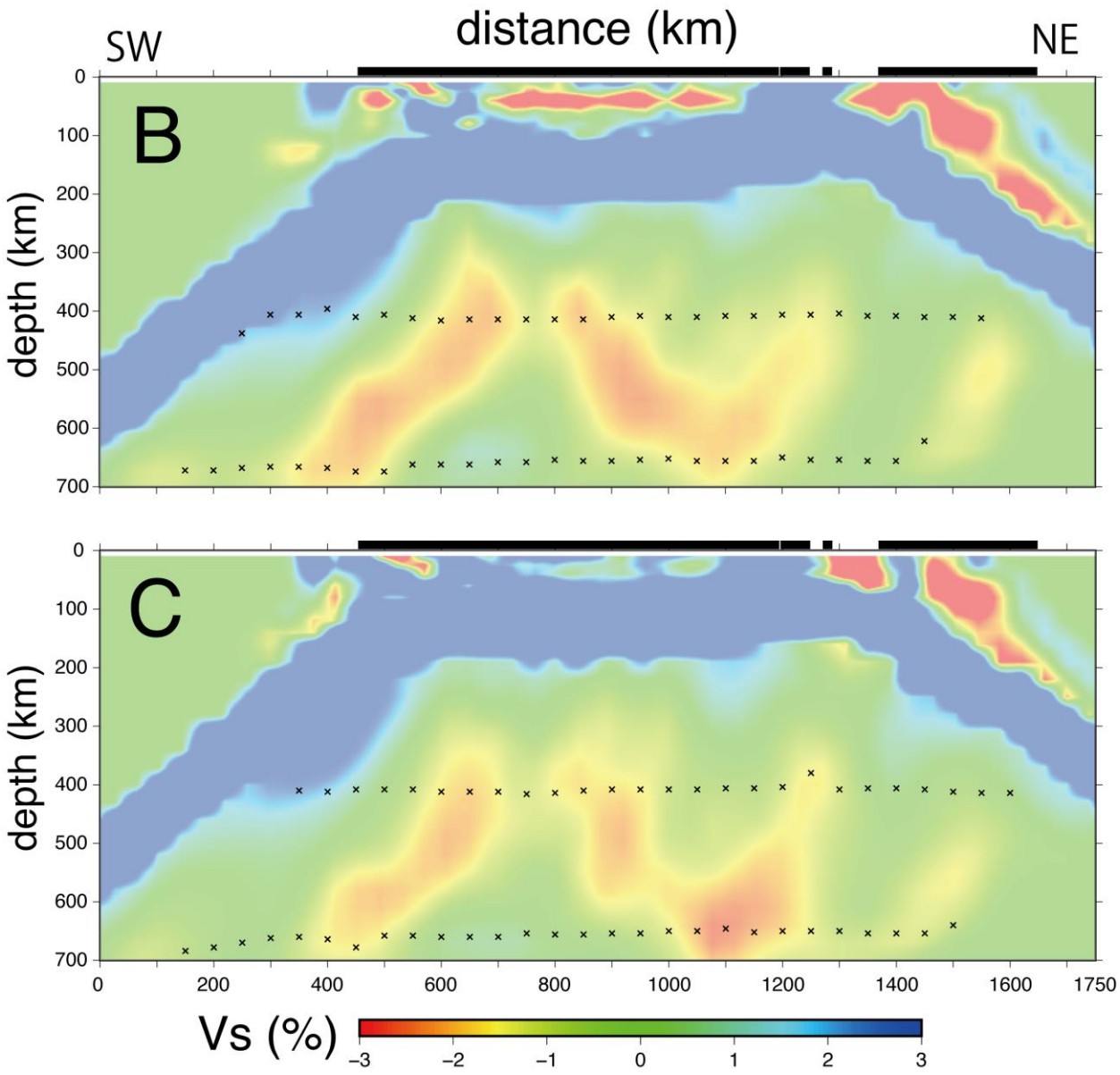

Figure 3. Vertical cross section of S-wave tomography along profile B and C obtained by Asamori and Zhao (2016). The red and blue colors denote low and high velocities, respectively. The black bar and cross marks are same as Fig 2. The crosses the depths of the 410 and 660 derived from RF images.

Another plausible cause of the sub-slab low-velocity anomaly is some degree of water contents. Mao et al. (2012) showed that water content of ~0.2 wt% can explain S-wave low velocity reduction of ~2 % observed in the mantle transition zone (Asamori and Zhao 2015; Wei et al., 2015; Liu and Zhao 2016). It is known that 1 wt% water content can shift the depth of phase transition of olivine at the 410 shallower by ~10 km (Smyth and Frost, 2002) and that of ringwoodite at the 660 deeper by 6~8 km (Higo et al., 2001; Litasov et al., 2005; Muir et al., 2021). Thus, the 0.2 w% water would elevate the 410 by ~2 km and depress the 660 by ~1.5 km,

given that the uplift of the 410 and depression of the 660 are proportional linearly to the water content. The possible depth changes of 410 and 660 caused by the water content of ~0.2 wt% are below the minimum resolution of RF imaging, which is controlled by the vertical grid spacing (2 km) used in this study. Therefore, we consider that the water content as small as ~0.2 wt% explains the two independent seismological observations: the amplitude of the sub-slab low-velocity anomaly and the little depth variation of the 410 and 660. The inferred water content of ~0.2 wt% is comparable to the water capacity of the lower mantle rock (~0.2–0.4 wt%) (Murakami et al.,2002), thereby being consistent with the observations that the sub-slab low-velocity anomaly originates from the lower mantle as suggested by tele-seismic tomography studies (Zhao 2004; Obayashi et al.,2015; Zhao 2015).

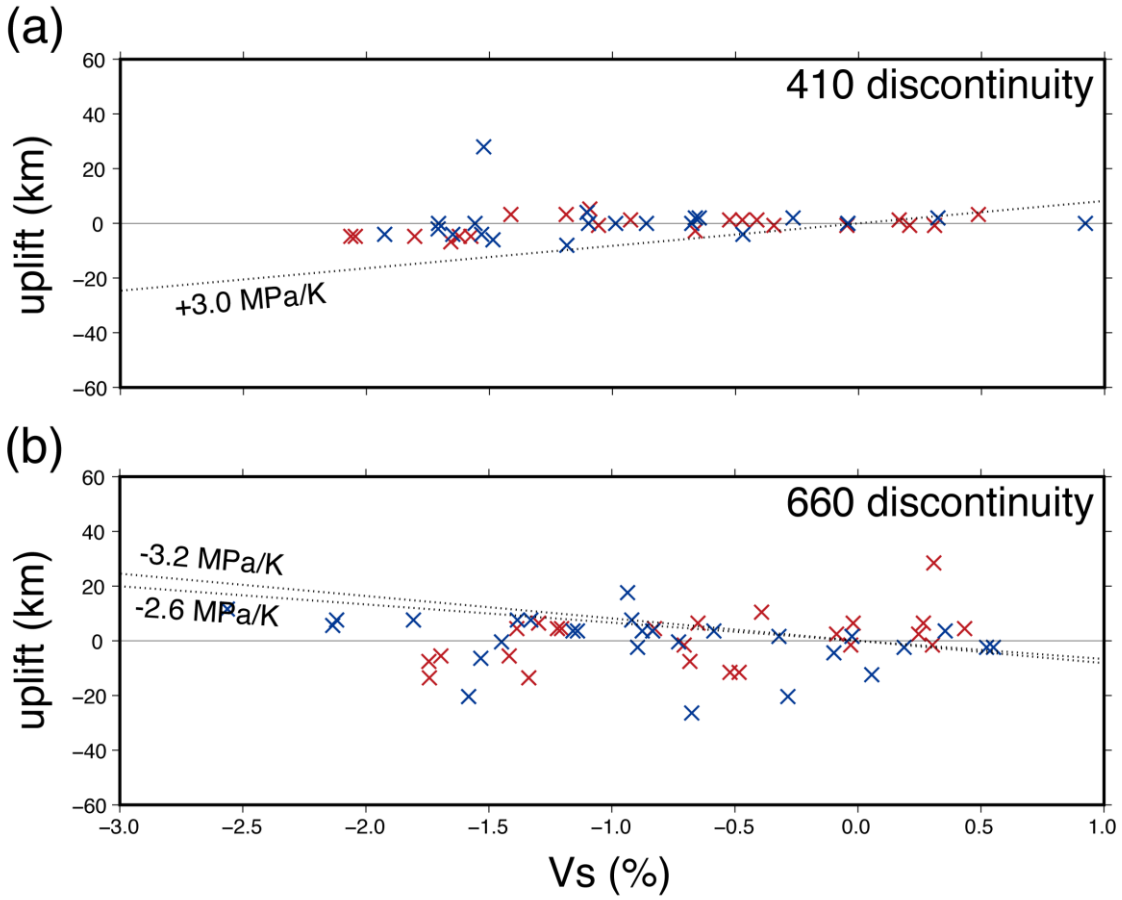

Figure 4. Scatter plots of the uplift of the (a) 410 and (b) 660 relative to the average depth along each of profiles B and C in Fig 1a versus S-wave velocity perturbation, which are taken from the cross marks in Figs 2 and 3. Red and blue symbols represent results for profile B and C, respectively. The dotted lines indicate the Clapeyron slope at the 410 (Bina and Helffrich 1994; Akaogi et al., 2007) and at the 660 (–2.6 MPa/K from Akaogi et al., 2007; –3.2 MPa/K from Muir et al., 2021). We assumed dlnVs/dT = 1%/ 100 K (Chiara et al., 2019) and density is 3.73 g/cm^3 at the 410 km and 3.99 g/cm^3 at the 660 km, respectively.

5 Conclusion

We determined the depth variation of the 410 and 660 discontinuities beneath northeastern Japan using RF imaging and revealed that the 410 and 660 are almost flat with no correlations with the sub-slab low-velocity anomaly. Therefore, it is unlikely that the sub-slab low-velocity anomaly results from high-temperature anomaly. We proposed that the sub-slab low-velocity anomaly corresponds to a wet plume originating from the lower mantle. The inferred water content of the plume is as small as ~0.2 wt%, which can explain both the flat 410 and 660 and ~2% S-wave velocity reduction in the sub-slab low-velocity anomaly.

The sub-slab wet plume model proposed in this study is different from conventional interpretations that the sub-slab low-velocity anomaly represents hot mantle materials (Morishige et al., 2010; Hawley et al., 2016; Portner et al.,2017; Bodner et al., 2018; Zhao and Hua 2021; Dai et al. 2023). Our results provide a new insight into the sub-slab mantle dynamics toward a better understanding mass circulation in the whole mantle.

Acknowledgments

We used waveform data obtained from Hi-net stations installed by National Research Institute for Earth Science and Disaster Resilience. We thank Dr. K. Asamori san for providing tomographic data, Dr. Y. Sawaki and Dr. T. Tonegawa for their advice in developing the receiver function analysis program, and Prof. S. Yoshioka and Prof. T. Kubo for useful discussions on the interpretation of receiver function images. This study was partly supported by JST SPRING, Grant Number JPMJSP2106, JSPS KAKENHI Grant Numbers JP20K20939, JP21H01176, and 21H01180, and by the Ministry of Education, Culture, Sports, Science and Technology (MEXT) of Japan, under its The Second Earthquake and Volcano Hazards Observation and Research Program (Earthquake and Volcano Hazard Reduction Research).

Open Research

The Hi-net sesmic waveforms (National Research Institute for Earth Science and Disaster Resilience, 2019) used in this study are publicly available at (https://hinetwww11.bosai.go.jp/auth/?LANG=).

References

Akaogi, M., Takayama, H., Kojitani, H., Kawaji, H., & Atake, T. (2007). Low-temperature heat capacities, entropies and enthalpies of Mg2SiO4 polymorphs, and α-β-γ and post-spinel phase relations at high pressure. *Physics and Chemistry of Minerals*, *34*(3), 169–183. https://doi.org/10.1007/s00269-006-0137-3

Anderson, O. L. & Isaak, D. G. (1995). Elastic constants of mantle minerals at high temperature. Mineral Physics & Crystallography. pp.64-97. https://doi.org/10.1029/RF002p0064

Asamori, K., & Zhao, D. (2015). Teleseismic shear wave tomography of the Japan subduction zone. *Geophysical Journal International*, *203*(3), 1752–1772. https://doi.org/10.1093/gji/ggv334

Bina, C. R., & Helffrich, G. (1994). Phase transition Clapeyron slopes and transition zone seismic discontinuity topography. *Journal of Geophysical Research*, *99*(B8). https://doi.org/10.1029/94jb00462

Bodmer, M., Toomey, D. R., Hooft, E. E. E., & Schmandt, B. (2018). Buoyant Asthenosphere Beneath Cascadia Influences Megathrust Segmentation. *Geophysical Research Letters*, *45*(14), 6954–6962. https://doi.org/10.1029/2018GL078700

Civiero, C., Custódio, S., Rawlinson, N., Strak, V., Silveira, G., Arroucau, P., & Corela, C. (2019). Thermal Nature of Mantle Upwellings Below the Ibero-Western Maghreb Region Inferred From Teleseismic Tomography. *Journal of Geophysical Research: Solid Earth*, *124*(2), 1781–1801. https://doi.org/10.1029/2018JB016531

Dai, Y., Rychert, C. A., & Harmon, N. (2023). Seismic Imaging Beneath Cascadia Shows Shallow Mantle Flow Patterns Guide Lower Mantle Upwellings. *Journal of Geophysical Research: Solid Earth*, *128*(9). https://doi.org/10.1029/2023JB026374

Dziewonski, A. M., & Anderson, D. L. (1981). Preliminary reference Earth model *. In *Preliminary reference Earth modeL Phys. Earth Planet. Inter* (Vol. 25). https://doi.org/10.1016/0031-9201(81)90046-7

Fan, J., & Zhao, D. (2021). Subslab heterogeneity and giant megathrust earthquakes. *Nature Geoscience*, *14*(5), 349–353. https://doi.org/10.1038/s41561-021-00728-x

Hawley, W. B., Allen, R. M., & Richards, M. A. (n.d.). *Tomography reveals buoyant asthenosphere accumulating beneath the Juan de Fuca plate*. https://doi.org/10.7932/NCEDC

Higo, Y., Inoue, T., Irifune, T., & Yurimoto, H. (2001). Effect of water on the spinel-postspinel transformation in Mg2SiO4. *Geophysical Research Letters*, *28*(18), 3505–3508. https://doi.org/10.1029/2001GL013194

Huang, Z., Zhao, D., & Wang, L. (2015). P wave tomography and anisotropy beneath Southeast Asia: Insight into mantle dynamics. *Journal of Geophysical Research: Solid Earth*, *120*(7), 5154–5174. https://doi.org/10.1002/2015JB012098

Kawakatsu, H., & Watada, S. (2007). Seismic evidence for deep-water transportation in the mantle. *Science*, *316*(5830), 1468-1471. https://doi.org/10.1126/science.1140855

Kawakatsu, H., & Yoshioka, S. (2011). Metastable olivine wedge and deep dry cold slab beneath southwest Japan. *Earth and Planetary Science Letters*, *303*(1–2), 1–10. https://doi.org/10.1016/j.epsl.2011.01.008

Kennett', B. L. N., & Engdah12, E. R. (1991). Traveltimes for global earthquake location and phase identification. In *Geophys. 1. Inf* (Vol. 105). https://academic.oup.com/gji/article/105/2/429/705789

Kennett, B. L. N., Engdahl, E. R., & Buland, R. (1995). Constraints on seismic velocities in the Earth from traveltimes. *Geophysical Journal International*, *122*(1), 108–124. https://doi.org/10.1111/j.1365-246X.1995.tb03540.x

Lee, H., Kim, Y. H., Bezada, M. J., & Clayton, R. W. (2023). The Role of Subslab Low-Velocity Anomalies Beneath the Nazca Ridge and Iquique Ridge on the Nazca Plate and Their Possible Contribution to the Subduction Angle. *Geophysical Research Letters*, *50*(23). https://doi.org/10.1029/2023GL106096

Liang, X., Zhao, D., Hua, Y., & Xu, Y. G. (2023). Mapping Mantle Flows and Slab Anisotropy in the Cascadia Subduction Zone. *Geophysical Research Letters*, *50*(23). https://doi.org/10.1029/2023GL105527

Litasov, K. D., Ohtani, E., Sano, A., Suzuki, A., & Funakoshi, K. (2005). Wet subduction versus cold subduction. *Geophysical Research Letters*, *32*(13), 1–5. https://doi.org/10.1029/2005GL022921

Liu, X., & Zhao, D. (2016a). P and S wave tomography of Japan subduction zone from joint inversions of local and teleseismic travel times and surface-wave data. *Physics of the Earth and Planetary Interiors*, *252*, 1–22. https://doi.org/10.1016/j.pepi.2016.01.002

Liu, X., & Zhao, D. (2016b). Seismic velocity azimuthal anisotropy of the Japan subduction zone: Constraints from P and S wave traveltimes. *Journal of Geophysical Research: Solid Earth*, *121*(7), 5086–5115. https://doi.org/10.1002/2016JB013116

Maeda, T., Obara, K., Furumura, T., & Saito, T. (2011). Interference of long-period seismic wavefield observed by the dense Hi-net array in Japan. *Journal of Geophysical Research: Solid Earth*, *116*(10). https://doi.org/10.1029/2011JB008464

Mao, Z., Lin, J. F., Jacobsen, S. D., Duffy, T. S., Chang, Y. Y., Smyth, J. R., Frost, D. J., Hauri, E. H., & Prakapenka, V. B. (2012). Sound velocities of hydrous ringwoodite to 16GPa and 673K. *Earth and Planetary Science Letters*, *331–332*, 112–119. https://doi.org/10.1016/j.epsl.2012.03.001

Morishige, M., Honda, S., Yoshida, M., Suetsugu, D., Bina, C., Inoue, T., Wiens, D., & Jellinek, M. (2010). Possibility of hot anomaly in the sub-slab mantle as an origin of low seismic velocity anomaly under the subducting Pacific plate. *Physics of the Earth and Planetary Interiors*, *183*(1–2), 353–365. https://doi.org/10.1016/j.pepi.2010.04.002

Muir, J. M. R., Zhang, F., & Brodholt, J. P. (2021). The effect of water on the post-spinel transition and evidence for extreme water contents at the bottom of the transition zone. *Earth and Planetary Science Letters*, *565*. https://doi.org/10.1016/j.epsl.2021.116909

National Research Institute for Earth Science and Disaster Resilience. (2019). NIED Hi-net [Dataset]. National Research Institute for Earth Science and Disaster Resilience. https://doi.org/10.17598/NIED.0003

Obayashi, M., Sugioka, H., Yoshimitsu, J., & Fukao, Y. (2006). High temperature anomalies oceanward of subducting slabs at the 410-km discontinuity. *Earth and Planetary Science Letters*, *243*(1–2), 149–158. https://doi.org/10.1016/j.epsl.2005.12.032

Portner, D. E., Beck, S., Zandt, G., & Scire, A. (2017). The nature of subslab slow velocity anomalies beneath South America. *Geophysical Research Letters*, *44*(10), 4747–4755. https://doi.org/10.1002/2017GL073106

Smyth, J. R., & Frost, D. J. (2002). The effect of water on the 410-km discontinuity: An experimental study. *Geophysical Research Letters*, *29*(10), 123-1-123–124. https://doi.org/10.1029/2001gl014418

Tonegawa, T., Hirahara, K., & Shibutani, T. (2005). Detailed structure of the upper mantle discontinuities around the Japan subduction zone imaged by receiver function analyses. In *Earth Planets Space* (Vol. 57). https://doi.org/10.1186/BF03351801

Wei, W., Xu, J., Zhao, D., & Shi, Y. (2012). East Asia mantle tomography: New insight into plate subduction and intraplate volcanism. *Journal of Asian Earth Sciences*, *60*, 88–103. https://doi.org/10.1016/j.jseaes.2012.08.001

Wei, W., Zhao, D., Xu, J., Wei, F., & Liu, G. (2015). P and S wave tomography and anisotropy in Northwest Pacific and East Asia: Constraints on stagnant slab and intraplate volcanism. *Journal of Geophysical Research: Solid Earth*, *120*(3), 1642–1666. https://doi.org/10.1002/2014JB011254

Zhao, D. (2004). Global tomographic images of mantle plumes and subducting slabs: Insight into deep Earth dynamics. *Physics of the Earth and Planetary Interiors*, *146*(1–2), 3–34. https://doi.org/10.1016/j.pepi.2003.07.032

Zhao, D. (2009). Multiscale seismic tomography and mantle dynamics. *Gondwana Research*, *15*(3–4), 297–323. https://doi.org/10.1016/j.gr.2008.07.003

Zhao, D., & Hua, Y. (2021). Anisotropic tomography of the Cascadia subduction zone. *Physics of the Earth and Planetary Interiors*, *318*. https://doi.org/10.1016/j.pepi.2021.106767

References From the Supporting Information

Dziewonski, A. M., & Anderson, D. L. (1981). Preliminary reference Earth model *. In *Preliminary reference Earth modeL Phys. Earth Planet. Inter* (Vol. 25). https://doi.org/10.1016/0031-9201(81)90046-7

337 Kennett', B. L. N., & Engdah12, E. R. (1991). Traveltimes for global earthquake location and
338 phase identification. In *Geophys. 1. Inf* (Vol. 105).
339 https://academic.oup.com/gji/article/105/2/429/705789
340 Kennett, B. L. N., Engdahl, E. R., & Buland, R. (1995). Constraints on seismic velocities in the
341 Earth from traveltimes. *Geophysical Journal International*, *122*(1), 108–124.
342 https://doi.org/10.1111/j.1365-246X.1995.tb03540.x
343
344